

Analysis and Modeling of Near-Field Effects on the Link Budget for UWB-WPAN Channels

Z. Irahauten, J. Dacuña, G.J.M. Janssen, H. Nikookar, A. Yarovoy and L.P. Ligthart
IRCTR/CWPC, Wireless and Mobile Communications Group,
Faculty of Electrical Engineering, Mathematics and Computer Science,
Delft University of Technology, Delft, The Netherlands
Email: Z.Irahauten@ewi.tudelft.nl

Abstract—Wireless personal area networks applications may benefit from the use of ultra-wideband (UWB) technology. In these applications transmit and receive antennas are very close to each other and the far-field condition assumed in most of the link budget models may not be satisfied. Under near-field conditions, variations in the link budget and pulse shape compared to the far-field can be observed. In this work, a new UWB link budget model for very short distances is proposed and validated with measurements using different types of antennas. The measurements have been performed in the time domain by exciting the antenna with very short pulse of 35 ps width covering a large frequency band. The proposed model, which includes frequency, antenna size and orientation as parameters, shows a good agreement with the simulations and the measurements.

I. INTRODUCTION

UWB is a promising technology for wireless personal area networks (WPAN) [1]. In WPAN applications, transmit and receive antennas can be very close to each other, i.e. within the near-field region. In this situation, the common link budget models are not valid because the behavior of the antennas is quite different from the behavior in the far-field. In the near-field region, however, different effects such as reactive fields, phase error, and even multiple reflections between the antennas may become important.

Several UWB measurement results for WPAN applications are reported in the literature [2]–[10]. In [3], the human body effect on UWB signal propagation is investigated, but only for the receive antenna near the body and with the transmit antenna in the far-field. In [4], UWB channel measurements for a Body Area Network (BAN) are presented where transmit and receive antenna are placed directly on the body and only the 3-6 GHz bandwidth was measured. Reference [6] shows the results of a set of time domain UWB measurements for very short distances. In spite of plenty of UWB measurement efforts for WPAN, the near-field effects on the link budget have not been analyzed.

In this paper, a novel UWB link budget model for WPAN applications is proposed and validated with measurements and simulations. The near-field effect and its consequences on the UWB-WPAN link budget are analyzed and its behavior

This research was supported in part by STW under the Green and Smart Process Technologies Program (Project 7976: Product Quality Control Using Smart PEAS Based UWB Technology).

is modeled. It turns out that known link budget models for the far-field can be applied but with some modifications. The structure of the paper is as follows. In section II, the near-field effect is analyzed. The link budget model is proposed and explained in section III. Section IV presents measurement results and verification of the proposed model. Concluding remarks are provided in section V.

II. NEAR-FIELD EFFECTS ANALYSIS

Different effects such as phase error, antenna mismatch (i.e. reactive fields) and even multiple reflections between the antennas can appear when transmit and receive antennas are close to each other. The phase error effect is associated to the fact that a spherical wave differs from a plane wave in a given fraction of wavelength λ (usually $\lambda/16$, or a phase error of $\pi/8$). When two antennas are close to each other, the rays of the spherical wave produced by the transmit antenna reach the receive antenna aperture with different phases. This affects the received power because the rays do not sum coherently. The phase of each ray is a function of the distance between antennas, the frequency and the dimension of the antennas. The antenna mismatch effect is restricted to distances smaller than $c/2\pi f_{min}$ [11] (where f_{min} is the minimum frequency). Since UWB is mainly introduced for indoor communications and the frequency band proposed by FCC for such environment is 3.1-10.6 GHz, the minimum distance is $c/2\pi f_{min} \approx 1.5$ cm. Thus, this effect will be negligible for most of the applications. The multiple antenna reflections mainly appear for large antennas which are not often used for WPAN applications. As a result, the link budget in the near-field will be primarily affected by the phase error. In this section, the near-field effect associated to the phase error is analyzed. Without loss of generality and for simplicity of the analysis a dipole antenna with a full matching has been assumed.

A. Phase error for a dipole

Let's assume the situation of a thin dipole as depicted in Figure 1(a). The parameter l is the length of the dipole, R is the position of a point source (infinitesimal dipole), $r(z)$ is the distance between the point source and every point of the dipole and α is the angle between the E -field and the z axis. The voltage in the terminals of the dipole as a function of the

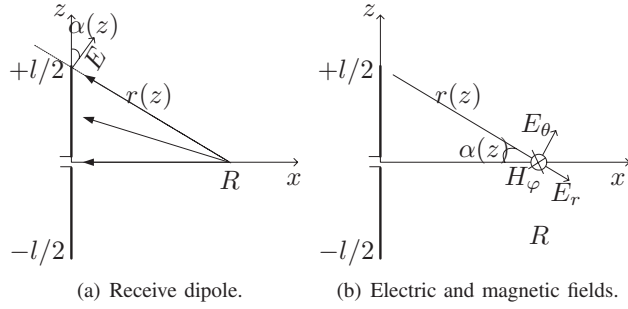


Fig. 1. Phase error for a dipole.

distance can be expressed as:

$$V \propto \int_{-l/2}^{+l/2} E_{rz}(z) I(z) dz \quad (1)$$

where $E_{rz}(z)$ is the z component of the electric field on the surface of the dipole and $I(z)$ is the current distribution on the surface of the dipole. For some constant c' , then:

$$V = c' \int_{-l/2}^{+l/2} I(z) \frac{e^{-jkr(z)}}{r(z)} \cos(\alpha(z)) dz = c' e^{-jkR} \int_{-l/2}^{+l/2} I(z) \frac{e^{-jk(r(z)-R)}}{r(z)} \cos\left(\arctan\left(\frac{z}{R}\right)\right) dz \quad (2)$$

where $k = 2\pi/\lambda$ is the wave number and z is the position along the dipole. Now, the voltage can be expressed as:

$$V = c'' \int_{-l/2}^{+l/2} I(z) \frac{e^{-j\frac{2\pi}{\lambda}(\sqrt{R^2+z^2}-R)}}{\sqrt{R^2+z^2}} \cos\left(\arctan\left(\frac{z}{R}\right)\right) dz \quad (3)$$

where c'' is a constant different from c' . Assuming both uniform and sinusoidal current distribution, the received power for several distances as a function of frequency for a 16 cm dipole is shown in Figure 2¹. The received power ($20 \log_{10}(V)$) is normalized to the distance assuming a distance dependence of $1/R^2$. From this figure it can be observed that the received power at very short distances is less than expected for the far-field region of the antenna. The main reason is that different rays picked up by the antenna are not in-phase, and therefore the total received power is less. Another reason is that when a source point is very close to the dipole, the rays of the received spherical wave have traveled a distance larger or equal to R . In the above formulas, the electric field radiated from an infinitesimal dipole is modeled as:

$$E_{\theta} \propto \frac{e^{-jkr}}{r} \hat{\theta}, \quad (4)$$

where $\hat{\theta}$ is a unitary vector in the θ direction. But actually, this is an approximation of the electric field for far-field regions. In the near-field this approximation is not valid and the total

¹Please note that a 16 cm dipole has been assumed here only to emphasize the effect and thus, the same effect can be observed for other dipole lengths.

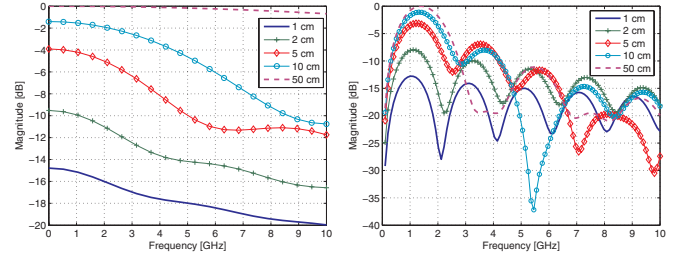


Fig. 2. Normalized received power vs. frequency for several distances, for a 16 cm dipole using: uniform (left), sinusoidal (right) current distribution.

electric field has to be considered using the equations for an infinitesimal dipole given by [11]:

$$E_r = \eta \frac{I_0 l \cos \theta}{2\pi r^2} \left[1 + \frac{1}{jkr} \right] e^{-jkr}, \quad (5)$$

$$E_{\theta} = j\eta \frac{k I_0 l \sin \theta}{4\pi r} \left[1 + \frac{1}{jkr} - \frac{1}{(kr)^2} \right] e^{-jkr}, \quad (6)$$

where I_0 is the excitation current, η is the free space impedance (120π), θ is the elevation angle with respect to the axis of the dipole assumed along the zenith, ϕ is the azimuth angle with respect to the x -axis in a rectangular coordinate system with its z -axis along the zenith, and r is the distance from the dipole. Considering the situation depicted in Figure 1(b), the electric and magnetic fields at R in the z and y (entering into the paper) directions are:

$$E_{rz} = \left[\int_{-l/2}^{+l/2} E_{\theta}(z) \cos(\alpha) dz + \int_{-l/2}^{+l/2} E_r(z) \cos\left(\frac{\pi}{2} - \alpha\right) dz \right] \hat{z} \quad (7)$$

$$H_{ry} = \left[\int_{-l/2}^{+l/2} H_{\phi}(z) dz \right] \hat{y} \quad (8)$$

Using the fields described in equations (5) and (6), the total electric and magnetic fields can be expressed as:

$$E_{rz} = \left[\int_{-l/2}^{+l/2} j\eta \frac{k I(z) l \sin \theta}{4\pi r(z)} \left[1 + \frac{1}{jkr(z)} - \frac{1}{(kr(z))^2} \right] e^{-jkr(z)} \cos(\alpha) dz + \int_{-l/2}^{+l/2} \eta \frac{I(z) l \cos \theta}{2\pi r(z)^2} \left[1 + \frac{1}{jkr(z)} \right] e^{-jkr(z)} \cos\left(\frac{\pi}{2} - \alpha\right) dz \right] \hat{z} \quad (9)$$

$$H_{ry} = \left[\int_{-l/2}^{+l/2} j \frac{k I(z) l \sin \theta}{4\pi r(z)} \left[1 + \frac{1}{jkr(z)} \right] e^{-jkr(z)} dz \right] \hat{y} \quad (10)$$

Using the above equations, the electric field as a function of the frequency for several points along the x axis are shown in Figure 3. It is observed that the normalized magnitude of the electric field decreases when the distance becomes smaller.

B. Phase error between two dipoles

In the previous section, the phase error effect for one dipole has been evaluated, when the source is a point source. In this section the same effect will be derived when transmit and

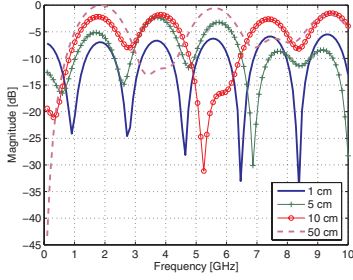


Fig. 3. Normalized magnitude of the electric field vs. frequency for different distances which are perpendicular to the axis of the dipole.

receive antenna are dipoles. Assuming the situation depicted in Figure 4, the voltage in the receive dipole is given by [11]:

$$V_{rx} \propto \frac{1}{I_{rx_i}} \int_{-l/2}^{+l/2} E_{rz}(z_{rx}) I_{rx}(z_{rx}) dz_{rx} \quad (11)$$

where I_{rx_i} is the current at the feed point of the receive antenna, V_{rx} is the voltage at the terminals of the receiving dipole, I_{rx} is the current illumination of the receive dipole, and z_{rx} is the position along the receive dipole. The electric field along the receive dipole is given by:

$$E_{rz}(z_{rx}) = \left[\begin{array}{c} \int_{-l/2}^{+l/2} E_{\theta}(z_{tx}, z_{rx}) \cos(\alpha(z_{tx}, z_{rx})) dz_{tx} + \\ \int_{-l/2}^{+l/2} E_r(z_{tx}, z_{rx}) \cos\left(\frac{\pi}{2} - \alpha(z_{tx}, z_{rx})\right) dz_{tx} \end{array} \right] \hat{z} \quad (12)$$

Substituting (5) and (6) in (12), the voltage in the receive antenna can be expressed as:

$$V_{rx} \propto \frac{1}{I_{rx_i}} \int_{-l/2}^{+l/2} \left[\begin{array}{c} \int_{-l/2}^{+l/2} \left(j\eta \frac{kI(z_{tx})l \sin \theta(z_{tx}, z_{rx})}{4\pi r(z_{tx}, z_{rx})} \right. \\ \left. \left[1 + \frac{1}{jkr(z_{tx}, z_{rx})} - \frac{1}{(kr(z_{tx}, z_{rx}))^2} \right] \right. \\ \left. e^{-jkr(z_{tx}, z_{rx})} \cos(\alpha(z_{tx}, z_{rx})) \right) dz_{tx} + \\ \int_{-l/2}^{+l/2} \left(\eta \frac{I(z_{tx})l \cos \theta(z_{tx}, z_{rx})}{2\pi r(z_{tx}, z_{rx})^2} \right. \\ \left. \left[1 + \frac{1}{jkr(z_{tx}, z_{rx})} \right] e^{-jkr(z_{tx}, z_{rx})} \right. \\ \left. \cos\left(\frac{\pi}{2} - \alpha(z_{tx}, z_{rx})\right) \right) dz_{tx} \end{array} \right] \cdot I_{rx}(z_{rx}) dz_{rx} \quad (13)$$

Figure 5(a) shows the normalized received power as a function of the distance between two dipoles using eq. (13). The power is integrated over the frequency band from 3 to 10 GHz. From this figure it can be seen that the received power at very short distances is less than expected for the far-field region of the antenna.

C. Simulation results

To validate expression (13), the obtained results of Figure 5(a) are compared to simulations. These simulations were

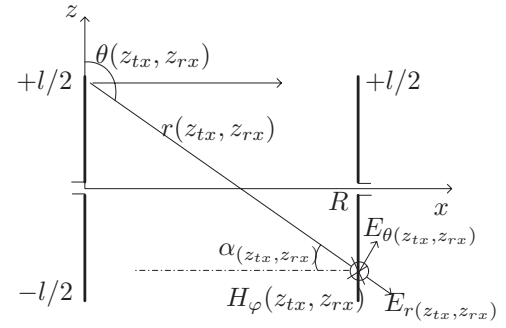


Fig. 4. Phase error between two dipoles.

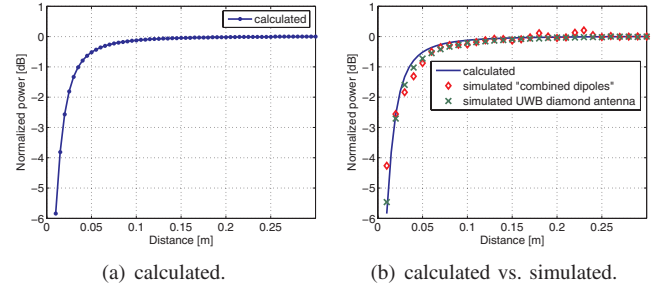


Fig. 5. Normalized received power, averaged over the frequency band 3 to 10 GHz, as a function of the distance.

done using the IE3D Electromagnetic simulator². As stated before, the calculations were made for a dipole antenna assuming a full matching. However, a dipole antenna is known as a narrowband antenna. Therefore, we simulated a kind of broadband dipole. This has been done by simulating different dipoles, matched for different discrete frequencies and the corresponding results are combined. Totally, 8 dipoles were simulated for several center frequencies: 3 to 10 GHz with a step of 1 GHz. Figure 5(b) shows the calculated and simulated normalized power, averaged over the frequency band (3-10 GHz), as a function of the distance between two dipoles. From this figure it can be seen that the calculations match well the simulations and they experience the same (exponential) behavior. Further, to validate whether the broadband dipole approach is correct or not, additional simulations with wide-band antennas have also been done. To this end, a diamond antenna has been simulated between 3 and 10 GHz and the results were compared to those of the broadband dipole in Figure 5(b). As is clear from this figure, the results match very well.

III. PROPOSED LINK BUDGET MODEL

As stated before, the link budget in the near-field is primarily affected by the phase error which is dependent on the considered bandwidth. When the received power is integrated over the large UWB bandwidth, it tends to be smaller than the expected received power using Friis law for the far-field, as can be seen from Figure 5. Moreover, the phase

²More details about the IE3D simulator is available at www.zeland.com

error becomes important when the physical dimensions of the antennas are large compared to the distance between the antennas. The distance at which this effect becomes important is $r < 2D^2/\lambda = r_{ff}$ [11] where D is the largest dimension of the antenna and r_{ff} is the far-field limit distance. The operating frequency also plays an important role because high frequencies will always have larger phase errors than lower frequencies for the same antenna dimensions and the behavior will be different for different frequencies, which means that it can result in signal distortion. Thus, these parameters should be considered in the modeling effort of the channel under near-field conditions. Modeling of near-field based on (13) is complicated. In this paper, we propose a simple model for the link budget in the near-field. The model considers an extra “near-field loss” term in addition to the “far-field loss”. In this model, the total loss can be expressed as:

$$L_{total}(r, f) = L_{ff}(r, f)\gamma_{nf}(r, f) \quad (14)$$

where

$$\gamma_{nf}(r, f) = 1 - e^{-\frac{r}{\delta_D(f, A_s, \theta)}} \quad (15)$$

L_{total} is the total loss of the channel, L_{ff} is the channel loss in the far-field, γ_{nf} is the correction factor due to near-field effects and δ_D is the distance decay constant which depends on the physical structure of the antenna A_s (i.e. dimensions, type), its orientation and the frequency. According to equation (15), for the far-field case $r \gg \delta_D$ the near-field correction factor $\gamma_{nf} \approx 1$. The proposed model is checked with the measurements performed using different types of antennas.

IV. MEASUREMENTS AND VERIFICATION

A. Measurement setup

In order to validate the proposed model, a set of measurements has been performed at different distances using a time domain technique. The generator fires a Gaussian-like pulse with a time duration of 35 ps. The sampling oscilloscope controls the sampling unit and the pulse generator with trigger pulses each 100 ms and has an operational bandwidth up to 26 GHz. An acquisition time window of 10 ns is used with 4096 points which means that the received signal is sampled at a rate of 1 sample per 2 ps. The antennas are placed on Styrofoam boards in order to keep them at more than one meter from the ground. Also there were no objects at less than one meter from the antennas. In this way, the reflections of the walls and/or objects can be removed using an appropriate time window. At transmit and receive sites two identical, vertically polarized, omni-directional antennas were used. One antenna was kept fixed while the other one was moved on a straight line covering a distance from 1 m to 0.5 cm. In total four pairs (4x2) different antennas were used: three pairs are bi-conical (BC) antennas with different sizes and referred as BC1, BC2 and BC3³, and one pair consists of Time Domain planar elliptical UWB (Schantz) antennas [12].

³The dimensions, [diameter, height] of these antennas in centimeters are: [16, 6.5], [7.5, 3.2] and [2.6, 0.8] for BC1, BC2 and BC3, respectively.

B. Data processing method

The received time domain signal is first filtered using a digital butterworth filter to suppress the out-of-band noise. Then, a raised cosine window is implemented to remove undesired signals and also to reduce the leakage problem when transforming the signal to the frequency domain. The received signal is normalized to the free space equation. Moreover, the measured signal at a given distance is de-convolved with a signal measured at far-field (e.g. 1 m). In this way, the modeling results do not depend either on the measurement system or the signal used to excite the channel which makes the proposed model easy to use in practice.

C. Measurement and Modeling results

Figure 6 shows the measurement results of the normalized received power as a function of the distance for different antennas. The distance decay constant δ_D is estimated using the least squares method. The loss due the near-filed effects can be seen as the difference between the curves and the horizontal 0 dB line. From this figure it can be observed that for all used antennas the extra loss due to near-field conditions decreases with the separation distance until r_{ff} , and it has an exponential behavior. The measurements and the proposed model match well for all antennas.

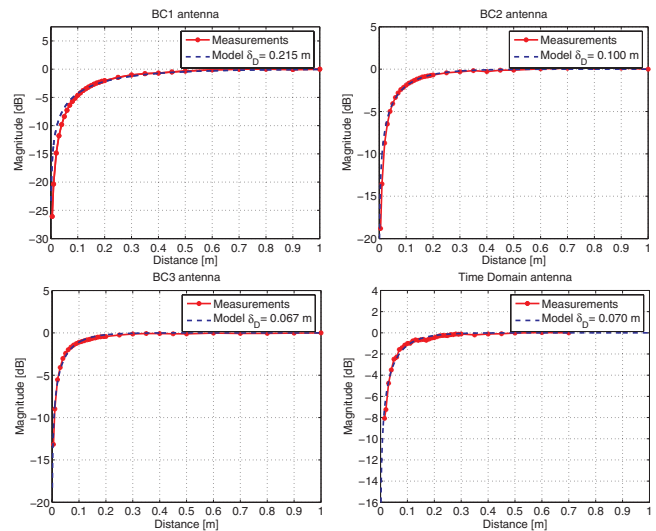


Fig. 6. Normalized link budget for the bi-conical and Time domain antennas.

It can also be concluded that for a fixed distance the losses are larger for large antennas and this agrees with the phase error effect which increases with the antenna dimension. The distance for which the extra loss is 3 dB is about 15 cm, 7.1 cm and 4 cm for the BC1, BC2 and BC3 antennas, respectively. These values are comparable with the maximum size of each antenna. Figure 7(a) shows δ_D as a function of the maximum antenna size A_s and its best fit model for the same type of antenna namely the bi-conical BC1, BC2 and BC3. Although, limited data was available, it can be generally observed that the behavior of δ_D tends to increase with A_s which agrees with the phase error definition. Moreover, the phase error will vary with

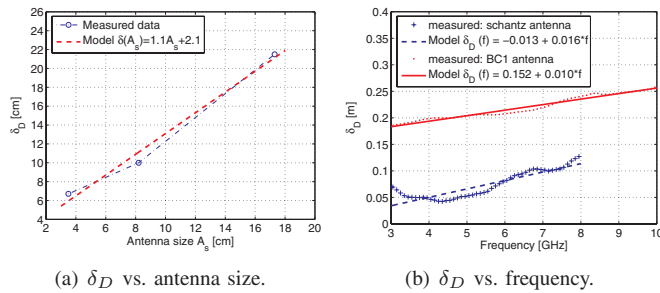


Fig. 7. Distance decay constant vs. maximum antenna size and frequency.

the operating frequency. To check this frequency dependency of the proposed model, the large bandwidth is divided into small frequency bands (i.e. chunks), and the model parameter δ_D is estimated for each chunk (e.g. 100 MHz). Figure 7(b) gives the measurement results of δ_D as function of frequency which show that δ_D increases slightly with frequency and the slope is almost the same for all cases. The parameter δ_D can be modeled as: $\delta_D(f) = a + bf$ where the constant a depends on the size of the antenna and the slope b depends on the geometry of the antenna.

For near-field measurements the radiation pattern of an antenna is not formed. Parameters as gain, directivity, etc have no meaning in this region because they are specifically defined assuming far-field conditions. However, since the phase error depends on the position of the antenna the model is checked for different antenna orientations. For this reason, additional measurements are performed keeping one antenna fixed while changing the orientation of the other antenna from -90 to $+90$ degrees with a step of 10 degrees. This is repeated for all distances between transmit and receive antenna using the Time Domain antennas. Figure 8(a) shows the measurement results of the normalized received power as a function of distance for different orientation angles. From this figure we can see that the proposed model is still valid for all orientation angles. Moreover, the loss at 0 degree is maximum. This can be explained by the fact that when the antenna is oriented at a certain angle, for example 90 degrees, a half of its aperture is situated more in the near-field region than the other half where its received power is higher and consequently the total power is higher. The behavior of δ_D as a function of θ is modeled in Figure 8(b).

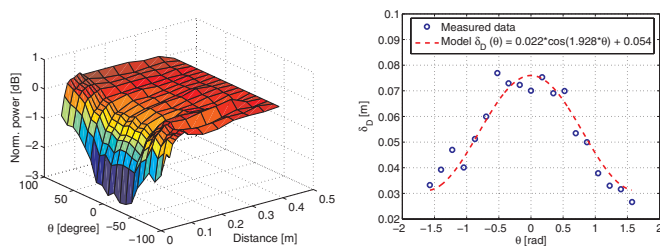


Fig. 8. The behavior of δ_D and its model with antenna orientation angle.

V. CONCLUSIONS

In this work, a new UWB link budget model for WPAN applications under near-field conditions of the antennas is proposed and validated by means of simulations and measurements. The model introduces a near-field modification factor to the far-field losses. The proposed model takes into account the phase error, which is the main near-field effect, and includes frequency, antenna size and orientation dependencies. A set of time domain UWB measurements covering a large frequency band (e.g. 3.1 to 10.6 GHz) was conducted using three different pairs of bi-conical antennas with different sizes and one pair of planar elliptical UWB (Schantz) antenna. The proposed model shows a good agreement with respect to the measurements and simulations. The near-field effect shows a strong dependency on the physical antenna size. This effect is stronger for larger antennas than for smaller antennas. The distance decay constant slightly increases with the frequency. The orientation angle affects the received power which is minimum at 0 degree for the planar antennas used.

REFERENCES

- [1] FCC, "Revision of part 15 the commission's rules regarding ultra-wideband transmission systems," *ET Docket*, 2002.
- [2] Y. Suzuki and T. Kobayashi, "Ultra wideband signal propagation in desktop environments," *IEEE Conf. on UWB Sys. and Tech.*, vol. 47, pp. 493–497, Nov. 2003.
- [3] T.B. Welch, R.L. Musselman, B.A. Emessiene, P.D. Gift, D.K. Choudhury, D.N. Cassadine and S.M. Yano, "The effects of the human body on UWB signal propagation in an indoor environment," *IEEE, JSAC*, vol. 20, no. 9, pp. 1778–1782, Dec. 2003.
- [4] T. Zasowski, F. Althaus, M. Stager, A. Wittneben and G. Troster, "UWB for noninvasive wireless body area networks: channel measurements and results," *IEEE Conf. on UWB Sys. and Tech.*, pp. 285–289, Nov. 2003.
- [5] C.C. Chong, Y. Kim, S.S. Lee, "A statistical based UWB multipath channel model for the indoor environments WPAN applications," *IEEE Proceedings on Intelligent Vehicles Symposium*, vol. 47, pp. 525–530, Jun. 2005.
- [6] Z. Irahhauten, J. Dacuña, G.J.M. Janssen and H. Nikoogar, "UWB channel measurements and results for wireless personal area networks applications," *The European Conference on Wireless Technology*, pp. 209–212, Oct. 2005.
- [7] S.S.M. Wong, F.C.M. Lau and C.K. Tse, "Propagation characteristics of UWB radio in a high-rise apartment," *The 8th Int Conf. on Adv. Comm. Tech. (ICACT)*, vol. 2, pp. 914–918, Feb. 2006.
- [8] K. Leechaikitjaroen, S. Promwong, P. Supanakoon, S. Chensirikul and S. Kaewmechai, "Indoor measurement results of UWB impulse radio for shot-range wireless systems with RMS delay spread and path loss," *IEEE Int. Sym. on Comm. and Inf. Tech. (ISCIT)*, vol. 1, pp. 684–688, Oct. 2005.
- [9] J. Choi, N-G. Kang, Y-S. Sung and S-C. Kim, "Empirical ultra wide band path loss model in office environments," *IEEE 63rd, Veh. Tech. Conf. VTC-spring*, vol. 4, pp. 1956–1960, Oct. 2006.
- [10] A. Fort, C. Desset, J. Ryckaert, P.D. Doncker, L.V. Biesen and S. Donnay, "Ultra wide-band body area channel model," *IEEE Int. Conf. on Comm. (ICC)*, vol. 4, pp. 2840–2844, May 2005.
- [11] C.A. Balanis, *Antenna theory: analysis and design*. Canada: John Wiley and Sons, 1997.
- [12] H.G. Schantz, "Bottom fed planar elliptical UWB antennas," *Ultra Wideband Systems and Technologies, IEEE Conference on*, pp. 219–223, Nov. 2003.